Algorithm for solving the equation of radiative transfer in the frequency domain

Kui Ren

Department of Applied Physics and Applied Mathematics, Columbia University, New York, New York 10027

Gassan S. Abdoulaev

Department of Biomedical Engineering, Columbia University, New York, New York 10027

Guillaume Bal

Department of Applied Physics and Applied Mathematics, Columbia University, New York, New York 10027

Andreas H. Hielscher

Departments of Biomedical Engineering and Radiology, Columbia University, New York, New York 10027

Received August 29, 2003

We present an algorithm that provides a frequency-domain solution of the equation of radiative transfer (ERT) for heterogeneous media of arbitrary shape. Although an ERT is more accurate than a diffusion equation, no ERT code for the widely employed frequency-domain case has been developed to date. In this work the ERT is discretized by a combination of discrete-ordinate and finite-volume methods. Two numerical simulations are presented. © 2004 Optical Society of America

OCIS codes: 000.4430, 170.0170, 170.3660, 170.5270, 170.7050.

Numerous studies concerning frequency-domain light propagation in tissues have been carried out since the early 1990s.[1–6] The term "frequency domain" refers to the case when the source intensity is modulated (typically at 100–1000 MHz), which leads to the propagation of so-called photon density waves in highly scattering media. A major application of these waves is in optical tomographic imaging, where it is commonly believed that frequency-domain techniques allow for better separation of absorption and scattering effects compared with steady-state methods. Currently available theoretical models for photon-density-wave propagation in random media are usually based on the diffusion equation,[1] which is an approximation to the more generally applicable equation of radiative transfer (ERT).[1,7] Although in many cases the diffusion theory is indeed a good approximation for light propagation in biological tissues, several researchers have theoretically and experimentally pointed out the limits of this approximation.[8–11] In trying to overcome these limitations, scientists have developed radiosity-diffusion models,[8] generalized diffusion models for specific cases,[11,12] and numerical methods for solving the full ERT directly.[13–15] However, to the best of our knowledge, no algorithm that solves the ERT in the frequency domain has been presented so far.

In the frequency domain the ERT in spatial domain D can be written as[1]

$$\left[\frac{i\omega}{v} + \Omega\cdot\nabla + \sigma_t(\mathbf{x})\right]\psi(\mathbf{x},\Omega,\omega) = \sigma_s(\mathbf{x})\int_{S^{n-1}} k(\Omega\cdot\Omega')\psi(\mathbf{x},\Omega',\omega)\mathrm{d}\mu(\Omega') + q(\mathbf{x},\Omega,\omega), \quad (1)$$

where $i=\sqrt{-1}$, $\mathbf{x}\in D\subset\mathbb{R}^n$ $(n=2,3)$ and $\omega\in\mathbb{R}^+$ are spatial position and modulation frequency, $v\in\mathbb{R}^+$ is the speed of light in the medium, $\Omega\in S^{n-1}$ (unit sphere of $\mathbb{R}^n$) is the direction of photon propagation, and $\mathrm{d}\mu$ is the Lebesgue surface measure normalized such that $\int_{S^{n-1}}\mathrm{d}\mu(\Omega)=1$. Nonnegative functions $\sigma_a(\mathbf{x})$ and $\sigma_s(\mathbf{x})$ are the absorption and scattering coefficients, respectively, and $\sigma_t(\mathbf{x})=\sigma_a(\mathbf{x})+\sigma_s(\mathbf{x})$. The unknown quantity, $\psi(x,\Omega,\omega)$, the radiance, is radiant power per unit solid angle per unit area perpendicular to the direction of propagation at $\mathbf{x}$ in the direction Ω at modulation frequency ω. The normalized kernel $k(\Omega\cdot\Omega')$ describes the probability that photons traveling in direction Ω' are scattered in direction Ω. $q(\mathbf{x},\Omega,\omega)$ is a volume source.

Within the framework of the discrete-ordinate method[16,17] the total scalar flux defined as the integration of $\psi(\mathbf{x},\Omega,\omega)$ over S^{n-1} is replaced by a weighted summation of the radiance field in different directions,[16]

$$\int_{S^{n-1}}\psi(\mathbf{x},\Omega,\omega)\mathrm{d}\mu(\Omega)\approx\sum_{j=1}^{J}\eta_j\psi(\mathbf{x},\Omega_j,\omega). \quad (2)$$

The transport equation is thus decomposed into a discrete set of J coupled differential equations that describe the photon flux field along J directions, i.e.,

$$\nabla\cdot(\Omega_j\psi)+\left(\sigma_t+\frac{i\omega}{v}\right)\psi(\mathbf{x},\Omega_j,\omega) = \sigma_s(\mathbf{x})\sum_{j'=1}^{J}\eta_{j'}k_{jj'}\psi(\mathbf{x},\Omega_{j'},\omega)+q(\mathbf{x},\Omega_j,\omega), \quad (3)$$

for $j=1,2,\ldots,J$, where $k_{jj'}=k(\Omega_j\cdot\Omega_{j'})$.

To further discretize the equations that result from the discrete-ordinate method, we use a finite-volume

0146-9592/04/060578-03$15.00/0 © 2004 Optical Society of America

method.[18] Finite-volume methods not only can handle complicated geometry by arbitrary triangulations but also conserve mass (or momentum, energy) in a discrete sense, which is important in transport calculations.

Let $\mathcal{M}$ be a mesh of $\mathbb{R}^n$ consisting of polyhedral bounded convex subsets of $\mathbb{R}^n$ that covers our computational domain D and let $\mathcal{E} \in \mathcal{M}$ be a control volume and $\partial\mathcal{E}$ be its boundary. Integrating the above discrete-ordinate equations [Eq. (3)] over control volume $\mathcal{E}$ yields

$$\int_{\partial\mathcal{E}} \Omega_j \cdot \mathbf{n}_{\mathcal{E}}(\mathbf{x})\psi^j \mathrm{d}\gamma(\mathbf{x}) + \int_{\mathcal{E}} \left[\sigma_t(\mathbf{x}) + \frac{i\omega}{v}\right]\psi^j \mathrm{d}\mathbf{x} = \int_{\mathcal{E}} \sigma_s(\mathbf{x}) \sum_{j'=1}^{J} \eta_{j'} k_{jj'} \psi^{j'} \mathrm{d}\mathbf{x} + \int_{\mathcal{E}} q^j \mathrm{d}\mathbf{x}, \quad (4)$$

for $j = 1, 2, \ldots, J$, where $\mathbf{n}_{\mathcal{E}}(\mathbf{x})$ denotes the outward normal to $\partial\mathcal{E}$ at point $\mathbf{x} \in \partial\mathcal{E}$, $\mathrm{d}\gamma(\mathbf{x})$ denotes the surface Lebesgue measure on $\partial\mathcal{E}$, and $\chi^j = \chi(\mathbf{x}, \Omega_j, \omega)$.

To obtain the finite-volume discretization equations, we assume that each of the control volumes is small enough so that we can take values of all space-dependent functions to be constant in the control volume. Together with an upwind scheme for the boundary flux [see Eq. (6) below], we arrive at the following equations:

$$\sum_{\kappa \in \partial\mathcal{E}} F^j_{\mathcal{E},\kappa} + \left[\sigma_t^{\mathcal{E}}(\mathbf{x}) + \frac{i\omega}{v}\right] V_{\mathcal{E}} \psi^j_{\mathcal{E}} = V_{\mathcal{E}} \sigma_s^{\mathcal{E}} \sum_{j'=1}^{J} \eta_{j'} k_{jj'} \psi^{j'}_{\mathcal{E}} + V_{\mathcal{E}} q^j_{\mathcal{E}}, \quad (5)$$

where the subscript (or superscript) $\mathcal{E}$ denotes the function value on control volume $\mathcal{E}$, and $V_{\mathcal{E}}$ is the volume of the control volume. An upwind scheme is applied to approximate flux F through the boundary of $\mathcal{E}$,

$$F^j_{\mathcal{E},\kappa} := \int_{\kappa} \Omega_j \cdot \mathbf{n}_{\mathcal{E}}(\mathbf{x})\psi^j \mathrm{d}\gamma(\mathbf{x}) = \begin{cases} S_{\mathcal{E},\kappa}\psi^j_{\mathcal{E}} & \text{if } S_{\mathcal{E},\kappa} \geq 0 \\ S_{\mathcal{E},\kappa}\psi^j_{\mathcal{E}'} & \text{if } S_{\mathcal{E},\kappa} < 0 \end{cases}, \quad (6)$$

where $\mathcal{E}'$ denotes the neighboring volume that has the common boundary κ with $\mathcal{E}$, and $S_{\mathcal{E},\kappa} := \int_{\kappa} \Omega_j \cdot \mathbf{n}_{\mathcal{E}}(\mathbf{x})\mathrm{d}\gamma(\mathbf{x})$.

Finally, after collecting the discretized transport equation [Eq. (5)] on all control volumes, we arrive at the following system of algebraic equations:

$$A\Psi = S\Psi + Q, \quad (7)$$

where A and S are discretized streaming-collision and scattering operators, respectively, and Q is a discretized source term.

To solve the system of equations [Eq. (7)] we adopt a source iteration technique,[17] for which we recast the system as

$$A\Psi^{l+1} = S\Psi^l + Q, \qquad l \geq 0. \quad (8)$$

The above equations are solved iteratively by a generalized minimal residual algorithm[19] until the convergence criterion $\|\Psi^l\|_{L^\infty} \leq 10^{-15}$ is satisfied.

To test the algorithm, we choose two examples. In the first example we consider a two-dimensional homogeneous medium of 5 cm × 5 cm, defined as $D := \{(x, y)^T \mid 0 < x, y < 5\}$. A point source is placed at $\mathbf{x}_s = (0, 2.5)^T$, and 49 detectors are uniformly distributed on the right boundary of the domain [see Fig. 1(a)]. The computational domain is discretized into 100 × 100 square cells. We use 128 directions (uniformly distributed on unit circle S^1) with equal weights. The scattering kernel is the Henyey–Greenstein phase function[17] with an anisotropic factor of $g = 0.9$. The computation takes approximately 10 min on a 500-MHz Pentium III processor.

In the second example we compare the results obtained for a cylindrical domain with and without a voidlike inclusion. By voidlike inclusion we mean a region in which both optical parameters are very small ($\sigma_a = 0.001\ \mathrm{cm}^{-1}$ and $\sigma_s = 0.01\ \mathrm{cm}^{-1}$). The domain is defined by $D := \{(x, y, z)^T \mid x^2 + y^2 < 1; 0 < z < 2\}$ and the void by $D_v = \{(x, y, z) \mid (x - 0.4)^2 + y^2 < 0.2^2, 0 < z < 2\}$. A point source is placed on $\mathbf{x}_s = (-1, 0, 1)^T$, and the detectors are uniformly distributed on the half-circle $\Gamma = \{(x, y, z) \mid x^2 + y^2 = 1, x \geq 0, z = 1\}$ [see Fig. 1(b)]. The domain is discretized into 11,836 tetrahedral elements, and 120 directions (S10) with full level symmetry[16] are used. Computations take approximately 40 min on a 500-MHz Pentium III processor.

In all computations the refractive index of the medium is constant and equals 1.37. Nonreentry boundary conditions[16] are applied. Furthermore, we define the complex flux through the domain boundary at point $\mathbf{x}$ with modulation frequency ω by

$$\phi(\mathbf{x}, \omega) = \int_{\Omega \cdot \nu(\mathbf{x}) > 0} \psi(\mathbf{x}, \Omega, \omega)\mathrm{d}\mu(\Omega), \quad (9)$$

where $\nu(\mathbf{x})$ is the outer normal of the domain boundary at $\mathbf{x} \in \partial D$. Since $\phi(\mathbf{x}, \omega)$ is complex valued, we define its amplitude I and phase θ through the relation $\phi(\mathbf{x}, \omega) = I(\mathbf{x}, \omega)\exp[i\theta(\mathbf{x}, \omega)]$, with θ chosen such that it vanishes in the vicinity of the source. If we

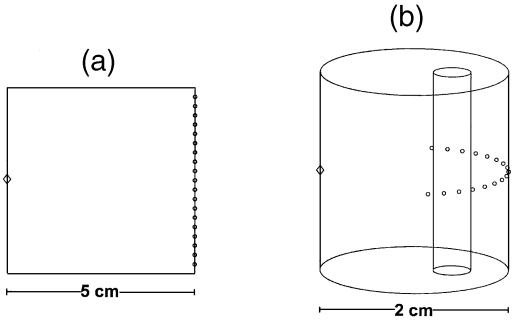

Fig. 1. Geometric settings of the computational domains. Diamond, source; circles, detectors.

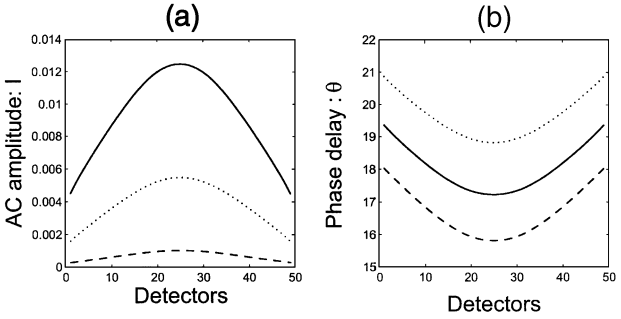

Fig. 2. (a) ac amplitude and (b) phase delay computed at the detectors for different optical parameters. Solid curve, $\sigma_a = 0.5\ \mathrm{cm}^{-1}$, $\sigma_s = 50\ \mathrm{cm}^{-1}$; dashed curve, $\sigma_a = 1.0\ \mathrm{cm}^{-1}$, $\sigma_s = 50\ \mathrm{cm}^{-1}$; dotted curve, $\sigma_a = 0.5\ \mathrm{cm}^{-1}$, $\sigma_s = 100\ \mathrm{cm}^{-1}$. The anisotropy factor $g = 0.9$ in all cases. The modulation frequency of the source is 200 MHz.

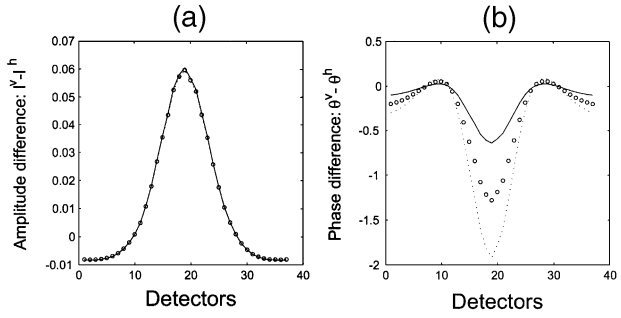

Fig. 3. Difference between (a) ac amplitude ($I^v - I^h$) and (b) phase delay ($\theta^v - \theta^h$) calculated at the detectors for various modulation frequencies in the domain with a void inclusion. $g = 0.9$ and 120 fully level-symmetric directions[16] are used. The optical parameters are $\sigma_a = 0.1\ \mathrm{cm}^{-1}$ and $\sigma_s = 120\ \mathrm{cm}^{-1}$. Solid curve, $\omega = 200$ MHz; circles, $\omega = 400$ MHz; dotted curve, $\omega = 600$ MHz.

set the phase of q to zero, then $\theta(\mathbf{x}, \omega)$ coincides with the so-called phase delay used in the frequency-domain literature.

Figures 2(a) and 2(b) show ac amplitude and phase delay for the first example calculated at detector positions assuming different optical properties. The modulation frequency for the source is taken to be 200 MHz. We observe that, at a fixed modulation frequency, an increase in either absorption or scattering will cause a decrease in the ac amplitude computed at the detectors [see Fig. 2(a)]. Phase delays obtained at the detectors [see Fig. 2(b)] increase with increasing scatter but decrease with increasing absorption. These observations agree with the underlying physics of the transport processes.[7]

Figure 3 shows results for the second example. We plot here the difference between the quantities calculated with and without the void inclusion as a function of detector positions. We assign the superscript v to those quantities computed in the former case and the superscript h to those in the latter case. We show the comparison at several modulation frequencies. It can be seen from Fig. 3 that the ac amplitude increases at the detectors right behind the void inclusion [Fig. 3(a)]. This well-known effect is due to the nonscattering and nonabsorbing nature of void regions. Furthermore, one can observe a change of phase that is becoming more pronounced as the modulation frequency of the source is increased [Fig. 3(b)].

In summary, we have presented an algorithm to solve the radiative transfer equation in the frequency domain with arbitrary geometries. The algorithm combines the discrete ordinate method with finite-volume discretizations. The scheme, although of first order, preserves the positivity of the transport solution.[7] Results for two numerical examples are in agreement with generally expected effects. Further testing with experimental data will be necessary to fully validate the code.

This work was supported in part by the National Heart, Lung, and Blood Institute (grant 2R44-HL-61057), which is a division of the National Institutes of Health. A. Hielscher's e-mail address is ahh2004@columbia.edu.

References

1. S. R. Arridge, Inverse Probl. **15,** R41 (1999).
2. D. M. Hueber, M. A. Franceschini, H. Y. Ma, Q. Zhang, J. R. Ballesteros, S. Fantini, D. Wallace, V. Ntziachristos, and B. Chance, Phys. Med. Biol. **46,** 41 (2001).
3. H. Jiang, K. D. Paulsen, U. L. Österberg, B. W. Pogue, and M. S. Patterson, Opt. Lett. **20,** 2128 (1995).
4. T. H. Pham, R. Hornung, H. P. Ha, T. Burney, D. Serna, L. Powell, M. Brenner, and B. J. Tromberg, J. Biomed. Opt. **7,** 34 (2002).
5. T. O. McBride, B. W. Pogue, S. Jiang, U. L. Osterberg, and K. D. Paulsen, Rev. Sci. Instrum. **72,** 1817 (2001).
6. R. Roy and E. M. Sevick-Muraca, Opt. Express **4,** 353 (1999), http://www.opticsexpress.org.
7. K. M. Case and P. F. Zweifel, *Linear Transport Theory* (Addison-Wesley, Reading, Mass., 1967).
8. S. R. Arridge, H. Dehghani, M. Schweiger, and E. Okada, Med. Phys. **27,** 252 (2000).
9. A. H. Hielscher, R. E. Alcouffe, and R. L. Barbour, Phys. Med. Biol. **43,** 1285 (1998).
10. A. D. Kim and A. Ishimaru, Appl. Opt. **37,** 5313 (1998).
11. G. Bal, SIAM (Soc. Ind. Appl. Math.) J. Appl. Math. **62,** 1677 (2002).
12. G. Bal and K. Ren, J. Opt. Soc. Am. A **20,** 2355 (2003).
13. O. Dorn, Inverse Probl. **14,** 1107 (1998).
14. A. D. Klose, U. Netz, J. Beuthan, and A. H. Hielscher, J. Quant. Spectrosc. Radiat. Transfer **72,** 691 (2002).
15. G. S. Abdoulaev and A. H. Hielscher, J. Electron. Imaging **12,** 594 (2003).
16. E. E. Lewis and W. F. Miller, *Computational Methods of Neutron Transport* (American Nuclear Society, La Grange Park, Ill., 1993).
17. M. L. Adams and E. W. Larsen, Prog. Nucl. Energy **40,** 3 (2002).
18. R. Eymard, T. Gallouet, and R. Herbin, in *Handbook of Numerical Analysis VII*, P. G. Ciarlet and J. L. Lions, eds. (North-Holland, Amsterdam, 2000).
19. Y. Saad and M. H. Schultz, SIAM (Soc. Ind. Appl. Math.) J. Sci. Stat. Comput. **30,** 856 (1986).